Papers

Climate of long internal waves and resuspension on the coastal shelf

OCEANOLOGIA, 50 (1), 2008.
pp. 5–21.

KEYWORDS
Internal waves
Turbulence
Instability
Resuspension

Darek J. Bogucki[1,*]
Larry G. Redekopp[2]

[1] Division of Applied Marine Physics, RSMAS,
University of Miami,
4600 Rickenbacker Causeway, FL–33149–1098 Miami, USA;

e-mail: DBogucki@rsmas.miami.edu

*corresponding author

[2] Department of Aerospace and Mechanical Engineering,
University of Southern California,
CL–90089–1191 Los Angeles, USA

Received 12 October 2007, revised 15 February 2008, accepted 19 February 2008.

Abstract

Observations of the shelf environment rarely associate internal solitary waves (ISWs) with the impact of their passage. An experiment observed during the Coastal Mixing and Optics 1996 (CMO '96), a sequence of long internal waves on a coastal shelf is reported, including both mode-1 and mode-2 waves, together with evidence related to the interaction of propagating ISWs and the benthic boundary layer. The observed ISW dynamics is shown to present a repetitive pattern or 'climate cycle'. The ISW-associated benthic signature described here occurs frequently (at least once a day) in the CMO '96 coastal area and suggests that ISWs under calm, summer-like conditions may have a decisive influence on the fate of near-bottom pollutants or biological processes in shelf regions.

The complete text of the paper is available at http://www.iopan.gda.pl/oceanologia/

1. Introduction

The bottom boundary layer in coastal regions and lakes comprises the interface between the sediment-laden seabed and the overlying water column, an interface across which active exchange of particles, chemicals and organisms occurs. An example of the pivotal importance of transport processes across the benthic boundary layer is the supply of iron from sediments to the water column. Iron is thought to limit biological productivity, and it has been proposed that continental-shelf sediments are the primary source of iron for coastal phytoplankton (Johnson et al. 1999). Consequently, processes which promote the flux of iron into the water column from the bottom boundary layer, such as internal wave-mediated resuspension, may significantly enhance productivity.

In the case of a shallow sea like the Baltic, the effect of benthic processes on the water column is more direct than on a relatively deeper continental shelf. In the case of Baltic Sea observations (Turnewitsch & Graf 2003) owing to the proximity of the chlorophyll *a* maximum to the bottom (chl *a* max at 15 m depth in 25 m deep water), energetic benthic processes can directly influence biological productivity by vertically mixing and 'diffusing' the chlorophyll layer.

In the classical framework, sediment resuspension is expected to occur when the speed of slowly varying currents above the benthic boundary layer increases above a threshold value, giving rise to enhanced shear stress on the seabed (Grant & Madsen 1986). Although this dynamics can contribute to significant dislodging and stirring of sediments, it is not clear that they necessarily act effectively as agents in transferring particulate matter to significant levels above the boundary layer. The basis for this statement is that the associated turbulent dynamics is almost certainly incoherent in space and time, and therefore expected to be of limited effectiveness in lifting sedimentary particles to significantly elevated levels above the boundary layer. Recent experimental evidence has challenged this traditional view of sediment resuspension. Bogucki et al. (1997) present evidence of the interaction of long internal waves with the bottom boundary layer in a specific case involving a bottom-trapped wave structure. Correlations of the episodic appearances of high concentrations of benthic material well above the boundary layer were made with the passage of such wave packets. Bogucki et al. (2005) present evidence of elevated particle concentrations in the near-benthic region following the passage of ISW (internal solitary waves) packets containing waves of depression. Hence, evidence is accruing that correlates elevated levels of benthic particle concentrations outside the wave-induced boundary layer with ISW packets of either polarity – depression or elevation. This correlation seems to occur when the adverse

pressure gradient imposed by the propagating internal wave exceeds the level required to stimulate break-up of locally separated regions in the wave-induced boundary layer (see Diamessis & Redekopp (2006)). (In general, an adverse pressure gradient occurs when the static pressure increases in the direction of the flow. This is important for boundary layers, since increasing the fluid pressure leads to a reduced kinetic energy and a deceleration of the flow – for a review, see Na & Moin (1998)).

The traditional view, where resuspension is related directly to the increased strength of mean currents, may be operative in some circumstances. However, it is an energetically costly mechanism and therefore likely to be quite rare. It requires the kinetic energy distributed across the whole water column to increase to sufficient levels to dislodge and resuspend bottom particles.

The passing ISW imposes vertical and horizontal scales on the current. These scales tend to decrease with higher internal wave modes. (For a general discussion of the internal wave modal structure, see, for example, Maslowe & Redekopp (1980) or Redekopp (2002)). Hence, the passage of an ISW packet can produce a low-frequency baroclinic current (for an example, see the Appendix, page 18). This current, if generated near the bottom, favors resuspension via a boundary layer eruption mechanism (Diamessis & Redekopp 2006). In such cases, a considerably reduced fraction of the energy needed in the case of barotropic flows might be sufficient to stimulate resuspension.

The above described vertical scale effect and the local pressure gradient effect can be expected to play important roles, especially when the ambient density stratification yields internal wave modes with horizontal currents exhibiting strong bottom trapping. We believe that the combination of these effects underlie the observed resuspension events evident in the data set discussed here.

We noted the effects and processes associated with passing ISWs during the 'nominal' (calm) and very energetic period of the Coastal Mixing and Optics (CMO) Experiment in 1996 in previous work (Bogucki et al. 2005). In contrast, the present work focuses only on the 'nominal' (calm) period of the CMO experiment (between Julian Days 238 and 246). We aim to expand on the effects of the passage of ISWs on the bottom boundary to better support the conjecture that internal wave-induced benthic eruptions may be a frequent occurrence in coastal shelf regions.

We report here the observation of both mode-1 and mode-2 ISWs in tidally-generated packets of long internal waves. Evidence for mode-2 ISWs in such packets has hitherto been scant at best. We believe that the observations of mode-2 ISWs in the shelf region presented here, together

with those reported in Bogucki et al. (2005), are among the first to provide conclusive evidence of their existence, suggesting that their appearance may in fact be frequent and widespread.

During the later stages of preparing this manuscript we became aware of another recent report of mode-2 ISWs in the analysis of the CMO data set (MacKinnon & Gregg 2005). Interestingly, we find that the appearance of mode-2 waves is closely connected with the presence of mode-1 waves and that their benthic stimulation (i.e., their creation of local boundary layer separation and subsequent eruption) can be as pronounced as that associated with mode-1 waves. The observations of the dynamics of mode-1 and mode-2 ISWs described here contain some common intrinsic features which we believe may also be relevant to the frequently occurring long internal wave motions in shallow seas and lakes (Saggio & Imberger 1998). For example, the results of recent measurements carried out in the Baltic Sea (Turnewitsch & Graf 2003) demonstrate the importance of ISW-related resuspension in shallow seas. During a 24-h long experiment, those authors (Turnewitsch & Graf 2003) documented the benthic effects of two semidiurnal ISW wave trains – see their Figure 6. At their experimental site, the total water column depth was approximately 25 m. The density stratification was as follows: an upper mixed layer (5–10 m), below that an approximately 15 m deep stratified layer, and a 5 m deep mixed bottom layer. They noted that the passage of each ISW resulted in enhanced vertical transport of chlorophyll *a* from the upper part of the water column down to the bottom layer and from the bottom turbid layer upward. Their dataset indicates that passing internal waves effectively control communication between the interior water column and sediment. In addition, their observations suggest that the 'internal wave climate' – in the form of a periodically generated ISW – could well be a frequent feature in the Baltic Sea.

2. The internal wave climate

The data presented in this paper are the results of the ONR[1]-sponsored Coastal Mixing and Optics 1996 (CMO) experiment. It was carried out on the 'Mud Patch' of the Middle Atlantic Bight, the southwestern portion of Georges Bank in the vicinity of 40°29.30′N, 70°30.28′W, 110 km south of Martha's Vineyard, Cape Cod, Massachusetts, U.S.A. A detailed description and appropriate reference to the experiment can be found in Bogucki et al. (2005). The water depth is approximately 70 m. The data were acquired from the central mooring (operated by Oregon State

[1]Office of Naval Research

University, OSU) (Boyd et al. 1997). The mooring contained a thermistor chain with thermistors spaced at 4 m intervals between 11 and 66 m, which provided temperature measurements at 16 depths every 2 minutes. An ADCP measured currents between 3 m and 55 m depth at 4 m intervals (Boyd et al. 1997) every 2 minutes.

The Super-BASS (maintained by the Woods Hole Oceanographic Institution, WHOI) (Shaw et al. 2001) made a few acoustic measurements per second of the local horizontal and vertical velocity between 0.38 meters above the bottom (mab) and 7 mab (Hill et al. 2001).

An optical tripod mooring (maintained by the University of California Santa Barbara, UCSB) (Dickey et al. 1998) provided the optical beam attenuation – beam-C measurement at 2 mab every 7.5 minutes. The two bottom tripods – Super-BASS and optical – were deployed approximately 400 m from the central mooring.

The time series shown in Figure 1 illustrates the general sequence observed during 'typical' summer conditions on the shelf. Figure 1a shows the time series of temperature at depths ranging between 26 to 51 m over a time period of approximately 5 days. The spikes (e.g., on Julian Day (JD) 243.1 or JD 243.7) are the fronts of ISW packets arriving at the mooring site. These waves propagate in a stratified wave guide with an upper stratified layer of 10 to 20 m thickness and an underlying weakly stratified layer (Figure 1h). The mode-1 distortions in the thermistor record correspond to waves of depression relative to the surface. A sequence of similar packets appears regularly throughout the time series, arriving essentially in phase with the tide.

A typical 'climate cycle' for a given packet is shown in the expansion of the thermistor time series between JD 243.1 to 243.65, a period of approximately 12 hours (Figure 1b). The 'climate cycle' started as the leading mode-1 ISW passed over the mooring on JD 243.1. The maximum vertical velocity (not shown) within 0.3 to 7 mab associated with the passing ISW was approximately 0.01 m s^{-1}, and the typical time scale of the high frequency vertical velocity fluctuations was 0.2 N^{-1}, where N is the maximum intrinsic frequency of the density stratification (around 0.03 s^{-1} – (Bogucki et al. 2005)). The peak horizontal current velocity within 7 mab was approximately 0.15 m s^{-1} (Figure 1d). Near-bottom particle concentrations increased concurrently with the leading mode-1 ISW as indicated by the beam-C signature, a measurement based on the attenuation of light at wavelength 660 nm over a 0.25 m path length. At the instrument depth of 2 mab, the beam-C signal is linearly dependent on the concentration of particles (Bogucki et al. 1997). The beam-C signature reached 0.6 m^{-1}, corresponding to quite a large concentration of particulate

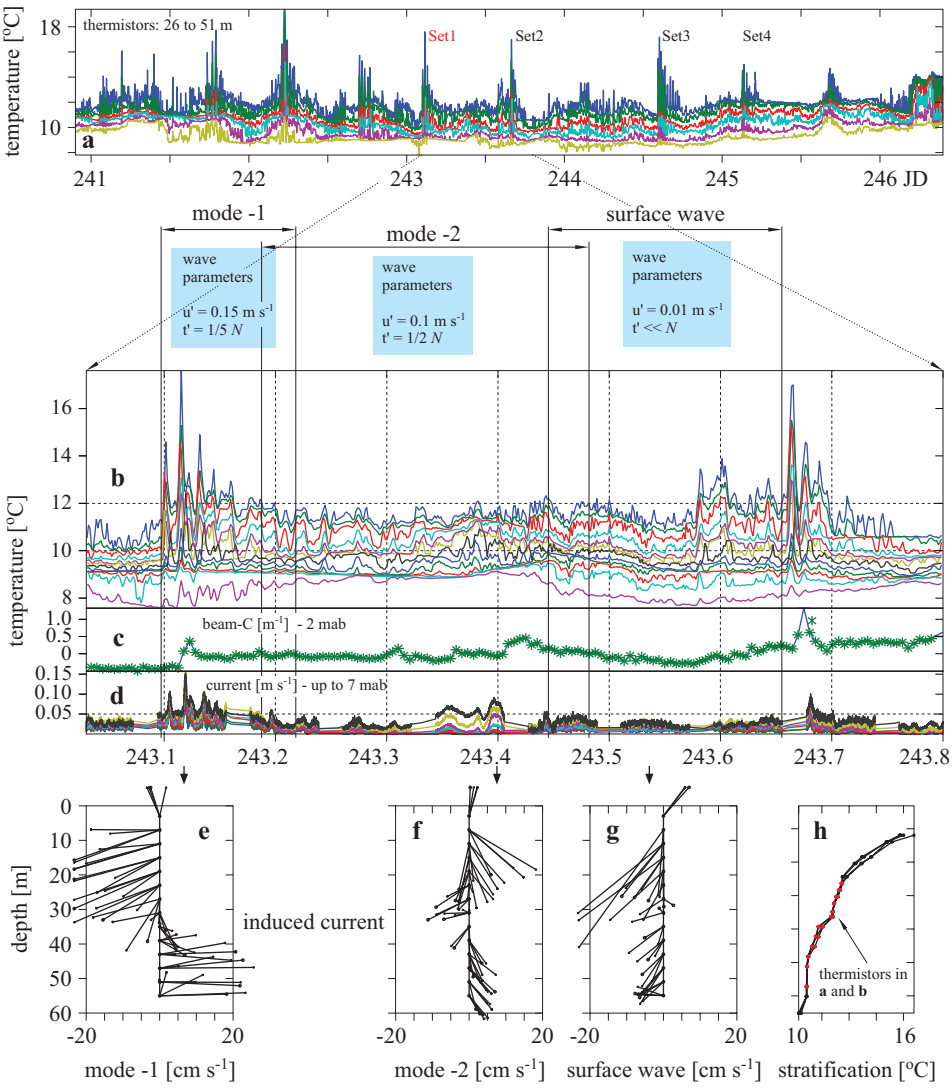

Figure 1. The typical internal wave climate on the shelf. (a) the five-day output from seven thermistors positioned between 26 to 51 m depth (positions shown in panel (h)). (b) expands the thermistor time series for a typical 'cycle' of ∼12 hours (here, JD 243.1 to 243.8). (c) shows the beam-C measured 2 meters above the bottom (mab). Panel (d) shows the wave-induced current measured between 0.3 to 7 mab. Panels (e), (f), and (g) show the fluctuating horizontal current field over the 0–60 m depth range (the average horizontal current for the time of a few N^{-1} has been subtracted) for selected snapshots corresponding to the three main periods of the climate. (h) shows the stratification and the thermistor location (denoted by red dots). The quantities inside the blue rectangle are wave-associated parameters observed in the mooring coordinate frame: u' – the values of the horizontal wave-induced velocity and t' – the associated wave passage time scale

matter at the sensor location (i.e., strong resuspension). The rise in beam-C signature coincident with the passage of the packet front is repeated with a fairly consistent frequency in the data record, although some exceptions have been noted (see the later discussion of Figure 2). The underlying reasons for these exceptions is not entirely clear, but we conjecture that co-propagating or counter-propagating barotropic currents can significantly mediate the requisite conditions for the appearance of elevated particle concentrations associated with a given wave-induced benthic stimulation; in some cases the benthic layer could have been removed and not yet restored.

The ISW packet had an amplitude (given by the maximum isopycnal displacement of 20 m below the water surface) of about 10–15 m, and generally traveled obliquely to the local current direction. Superimposing the wave-induced velocity onto the projection of the tidal current along the packet trajectory occasionally led to the appearance of reversed flow in the footprint of the wave packets.

In the 'climate cycle', the mode-1 wave was dominant until approximately JD 243.2, when the modal structure of the disturbances passing over the mooring changed gradually to mode-2 over a time interval of about an hour. (For a discussion of mode-2 properties and induced horizontal current, see the Appendix, p. 18). By JD 243.25 mode-2 waves dominated the vertical structure of the disturbance field. The vertical distribution of the horizontal current (without any attempt to remove any fraction of the mode-1 waves) (Figure 1f) clearly shows the significant contribution of the mode-2 structure. The induced horizontal current was of the order of 0.1 m s^{-1} (Figure 1d), the fluctuations in vertical velocity were of the order of 0.005 m s^{-1}, and the characteristic time scale was 0.5 N^{-1}.

Mode-2 waves generally appear as wide features on the time series, approximately twice as wide as mode-1 waves, due to their lower wave speed. However, it is the wavelength that sets the gradient impressed on the benthic layer; the wave speed only controls the residence time of the wave as it passes a fixed location. At JD 243.38 the mode-2 wave was large enough to reverse the near-bottom current and to initiate sediment resuspension (examples are cited in Figure 2).

After JD 243.4 the horizontal disturbance velocity shows the presence of a mode-2 wave with some contamination from the surface wave field. By JD 243.45, the surface wave field in the 'climate cycle', with its familiar exponential decay with depth, induced high-frequency variations (corresponding to the surface wave frequency) of the near-bottom current (Figure 1d). The surface wave amplitude was around 1 m at that time (Chang et al. 2001). The corresponding near-bottom (7 mab) horizontal velocity fluctuations were approximately 0.01 m s^{-1} and the characteristic

time scale was much shorter than N^{-1}. Typically the mode-1 or mode-2 horizontal induced wave speeds were around 0.1 m s^{-1} or more – for a discussion, see the Appendix – Figure 3, p. 19. The relatively incoherent action of the surface wave field, its higher frequency and smaller magnitude fluctuations, were not conducive to generating the near-bottom flow structure at the required time and space scales needed for efficient resuspension.

How frequent is this internal wave 'climate cycle'? The answer to this question is addressed by examining the data sets shown in Figure 2. Similar wave climate characteristics were observed for nearly every internal wave packet during the period JD 241 till JD 246. The data corresponding to JD 243.1 to JD 243.6 are displayed in Figure 1 and labeled as Set1, while other consecutive cases are labeled as Set2, Set3, and Set4 shown in Figure 2. For example, Set2 contains observations for the tidal cycle following Set1.

The observed increase in near-bottom particulate load is associated with mode-2 waves for Set2, Set3 and Set4. Curiously enough, the mode-1 waves, albeit stronger in terms of induced current, do not always induce resuspension, as in Set3 and Set4, for example. This can be attributed to the complex interplay between the ISW-induced current and the background current (nominally defined as the horizontal current averaged over a scale in excess of the internal wave packet scale). Also, a stronger current does not necessarily imply a stronger adverse pressure gradient in the lee of a trough of depression. An enhanced beam-C signature only seems to result when the near-bottom current is sufficiently decelerated beyond the threshold level, implying the strong likelihood of boundary layer separation stimulated by a wave-forced adverse pressure gradient. Based on recent model studies, (Wang & Redekopp 2001, Diamessis & Redekopp 2006) the strength of the adverse pressure gradient required for dynamic eruptions of the wave-induced boundary layer was found to depend on both the modal eigenstructure and the magnitude and direction of larger-scale currents, i.e., the actual spatially varying current at the outer edge of the boundary layer.

Figure 2. Selected data for Set2, Set3 and Set4. Set2 – The mode-1 associated beam-C increase occurs at JD 243.655 (upper panel). (The leading mode-1 wave with impression on the thermocline is shown in Figure 1). The mode-2 induced current is shown in the lower panel at JD=243.8. Set3 – The mode-1 wave induced current structure is shown (at T=244.6). The mode-1 wave does not appear to increase the particulate load. After JD 244.6, the near-bottom (at 0.38 mab and 7 mab) current changes direction three times in response to passing ISW. This results in a near-bottom particulate concentration increase. The mode-2 wave-induced current structure is shown for JD=244.665. Set4 – The mode-1 passage on JD=245.2 does not increase the particulate load. Mode-2 passage on JD=245.4 (wave induced vertical velocity shown) results in an increase of the near-bottom particulate load

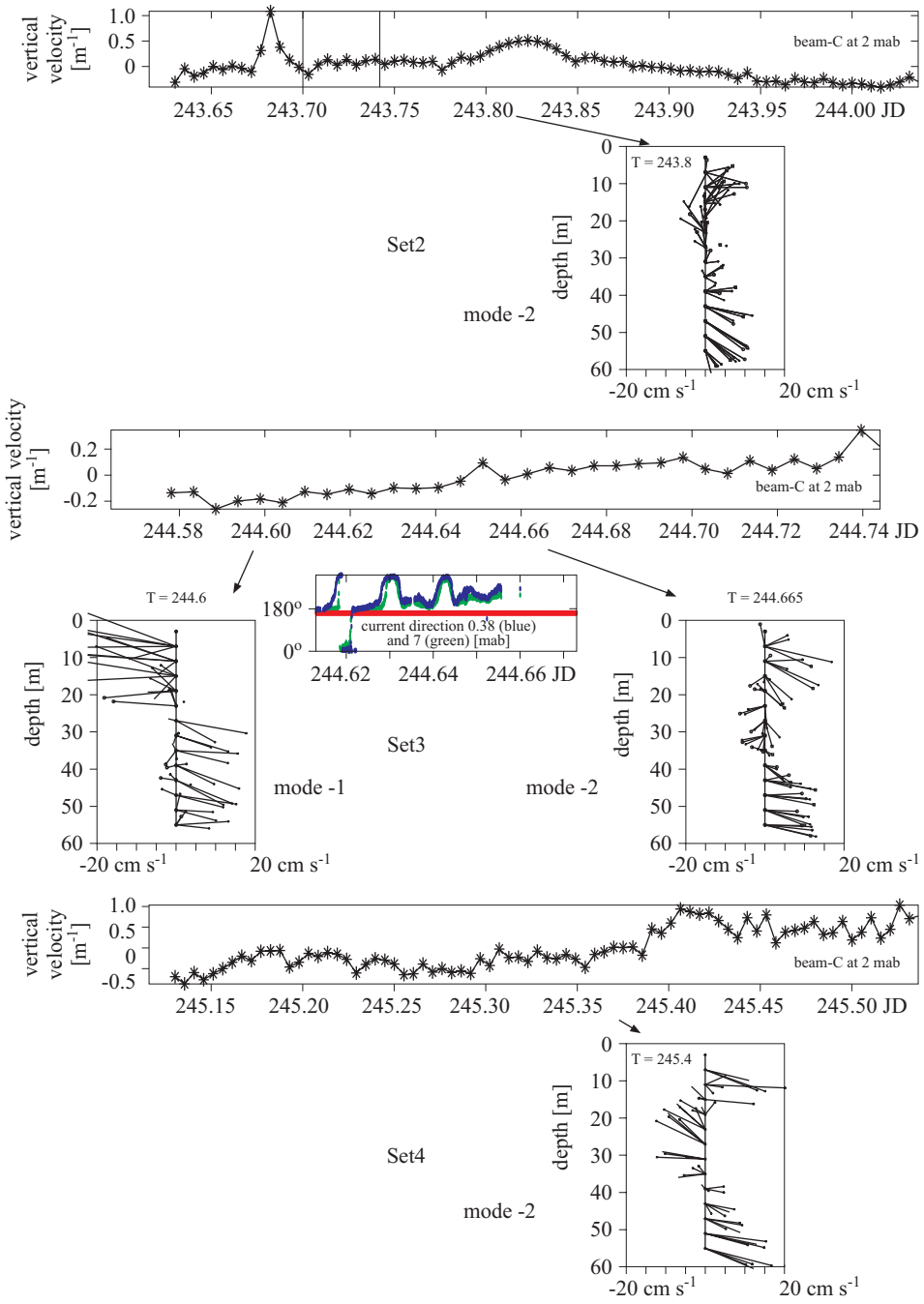
vertical velocity [m-1]
1.0
0.5
0
beam-C at 2 mab
243.65 243.70 243.75 243.80 243.85 243.90 243.95 244.00 JD
T = 243.8
depth [m]
Set2
mode -2
-20 cm s-1
20 cm s-1
vertical velocity [m-1]
0.2
0
-0.2
beam-C at 2 mab
244.58 244.60 244.62 244.64 244.66 244.68 244.70 244.72 244.74 JD
T = 244.6
T = 244.665
180o
0o
current direction 0.38 (blue) and 7 (green) [mab]
244.62 244.64 244.66 JD
depth [m]
Set3
mode -1
mode -2
vertical velocity [m-1]
1.0
0.5
0
-0.5
beam-C at 2 mab
245.15 245.20 245.25 245.30 245.35 245.40 245.45 245.50 JD
T = 245.4
Set4
mode -2

Figure 2.

Mode-2 waves often have an eigenfunction structure that possess a stronger bottom trapping of the wave-induced horizontal velocity, plus a shorter wavelength than mode-1 ISWs (see the Appendix – Figure 3), both of which conspire to more readily induce local flow separation in regions of adverse pressure gradients. An example of such characteristics is depicted in the inset to the Set3 data shown in Figure 2. The near-bottom flow direction of the full measured velocity field is shown just prior to a progressive rise in the beam-C signature. There are two, clearly visible cycles of flow reversal shown (i.e., a 180 degree change in flow direction) that reach at least to the level of 7 mab. Flow reversals of this nature generally precede (or are nearly coincident with) marked increases in the beam-C signal. Such coincidences argue for resuspension via a local dynamics as opposed to the appearance of particulate matter being advected past the measurement station that was derived from some unidentified process occurring at an upstream site.

The 'climate cycle' delineated here starts with a mode-1 dominance, is followed by a mode-2 dominance, and then by a subsidence of the long internal wave field to a level where the disturbance field is dominated by surface waves. The strength of the near-bottom current is largest under mode-1 waves at the front of the ISW packet. Near-bottom current strengths decline as mode-2 waves appear, and finally reach a minimum associated with surface wave 'noise'. However, the generation of local regions of adverse pressure gradient may, in some circumstances, be more pronounced when mode-2 waves dominate the disturbance field.

Why are the ISWs so effective in resuspension? We believe that the particle concentration profile near the seabed, on average, reflects an equilibrium with the energetics of surface wave action. Typical mode-1 or mode-2 ISWs induce benthic currents that occur episodically and are usually above the surface wave 'noise' level. ISWs are, therefore, potential drivers for significant benthic stimulation, even resuspension of benthic particles. An important point of the present analysis of the several internal wave 'climate cycles' is the existence of internal wave mode coupling: mode-1 waves are (frequently) followed by mode-2 waves as the mode-1 dominated front of the packet passes. Furthermore, internal wave-mediated resuspension occurs under both mode-1 dominated and mode-2 dominated portions of the climate. Based on model studies (e.g., Diamessis & Redekopp 2006), strong eruptions of the wave-induced benthic boundary layer are directly linked to a near-bottom structure of the current (ambient plus ISW-induced) that renders the flow susceptible to an intrinsic ('global') instability. These model studies point to the pivotal role of the wave-generated pressure gradient impressed on the benthic layer.

In the present context ISW packets impose an alternating pressure gradient field which is of reasonably large scale relative to the water column depth, and one whose strength increases quite strongly with wave amplitude. The surface waves also impose alternating pressure gradient fields on the benthic layer, but as such they also have the potential to release a similar dynamics. However, the pressure gradients associated with surface waves alternate with substantially higher frequencies than those arising under long internal waves (but a much smaller horizontal pressure gradient – as compared to mode-2 ISW – see the Appendix, p. 18), and they also have a strength that diminishes quite rapidly with depth (except for very long waves whose frequency is also low). Hence, surface waves generally exert a much weaker pressure gradient on benthic layers.

For example, the corresponding horizontal pressure gradient or equivalent horizontal velocity gradient (via Bernoulli's equation) associated with high frequency (one wave every 10 sec) at 7 mab is around 0.01 m s^{-1} (see Figure 2d) for a 300 m long wave (Shaw & Trowbridge 2001). For a 7.5 m long wave of mode-2 ISW this horizontal velocity gradient is over 0.16 m s^{-1} with a much lower corresponding frequency of around 1/(tens of minutes). Hence, the mode-2 ISW induced horizontal pressure gradient impressed on the boundary layer is larger by a factor of 640 (!) or more than one for a dominant surface wave.

Also, the surface wave frequency is sufficiently high compared to the intrinsic growth rate required for boundary layer instabilities to grow to levels that lead to boundary layer eruption. In contrast, the wave-induced boundary layer in the footprint of an ISW packet naturally creates conditions favorable to the release of the intrinsic instability that causes a large-scale eruption of the boundary layer. As such, an internal wave packet has the capacity to initiate measurable resuspension, and that simultaneously generates a dynamics (i.e., a rising assemblage of coherent vortex structures) which facilitates transport of particulate matter away from the bottom. This capacity for resuspension and transport depends on a complex interplay between the wave-induced current and the strength and directionality of ambient tidal or mesoscale currents. Episodes of measurable enhancements in particulate concentration seem to be linked to local generation of separated flow in the wave-induced boundary layer (manifested by flow reversals shown in Figure 2, Set3) arising from wave-generated, local regions of adverse pressure gradient.

3. Conclusions

The ISW's 'climate cycle' occurs at semi-diurnal to diurnal frequency (Figure 1a). Although the precise trigger of these episodic events is beyond

the scope of this study, we believe that tidal forcing interacts regularly with the background current field to generate events with time series quite similar to those shown in Figure 1. In six of the eight events shown on Figure 1a, beam-C rose above the immediately-prior background level by more than 50%. The beam-C signature varies widely in time (and probably somewhat in space depending on background currents), and an average beam-C signature associated with a continuous long-term time series fails to reveal the 'climate cycle' resuspension events that give rise to and dominate the vertical transport of bio-geochemical particulates. Further examination of the complete data record of six months (Bogucki et al. 2005) indicates that these cycles, accompanied by episodes of resuspension, consistently recur under quiescent conditions, thus constituting the background 'climate'. SAR imagery indicates that they can be expected to occur over considerable sections of the shelf.

We suggest, therefore, and present direct evidence obtained from a continuous record spanning several days, that benthic stimulation leading to episodes of resuspension occur in concert with the appearance of energetic packets of long ISWs. Since prominent benthic resuspension occurs only episodically, the episodes of resuspension are apparently triggered by an induced, near-bottom flow structure favoring dislodgement and vertical transport of benthic particles only when a threshold condition is exceeded. Benthic resuspension, mixing, and transport are therefore decidedly event driven and not a consequence of a continuous, nominal process. Furthermore, these events occur repetitively to make up a background 'climate', which can be interrupted or enhanced by remote or local forcing effects such as large-scale, energetic storms.

The most promising candidate for a dynamic mechanism underlying the observed resuspension events is the onset of an intrinsic instability that occurs when certain threshold conditions are exceeded. Evidence for the spontaneous onset of such an instability in wave-induced boundary layers, widely termed 'global instability', is delineated in linear instability analysis (Hammond & Redekopp 1998), and in direct numerical simulations presented by Wang & Redekopp (2001) and Diamessis & Redekopp (2006). As detailed in Diamessis & Redekopp (2006), the early onset of global instability (which occurs in a time developing boundary layer relative to the frame of a single, fixed measuring station) is reflected in the presence of upstream and downstream propagating instability waves inside the thin, attached boundary layer. Disturbances with such frequency within a thin layer are not discernible in the resolution of the present measurements, even at the 0.38 mab level. What is also clearly seen in the simulations is a distinct reversal of the flow within the thin boundary layer prior to onset of

the instability, as depicted in the data shown in Figure 2. Furthermore, the simulations reveal that the development of global instability is indeed rapid on time scales based on the IW phase speed and fluid column depth, leading to the quite sudden eruption of a thin, wave-induced viscous layer. The appearance in the present time series of flow reversal, even extending to the 7 mab level, correlated across the erupted layer and varying temporally with a scale commensurate with the relevant long-wave phase speeds, comprises the most definitive characteristic of the likely action of global instability evident in the time series presented here. The onset of global instability in the footprint of an ISW imposes a shorter-scale, coherent horizontal structure on the benthic layer that significantly enhances both horizontal and vertical gradients, thus endowing the flow with a greater potential for dislodging and lifting benthic particles. Furthermore, this global instability imposes a strong space-time coherence on the ensuing dynamics, as opposed to a random smaller-scale stirring associated with the broadband, incoherent flow within most turbulent boundary layers. Additionally, the coherent vortex structures generated during the eruption of the benthic layer rise considerably above the nominal boundary layer thickness. Thus, they facilitate the lifting of seabed particles to much greater heights above the bottom where they can be transported both horizontally and vertically by stronger and larger-scale interior motions.

The preliminary evidence presented here (see Figure 2) of flow reversal occurring near the bottom under certain wave conditions, and the concurrent increase in the concentration of suspended particles (i.e., beam-C), is consistent with our hypothesis that the onset of global instability is responsible for ISW-mediated resuspension. Evidence is accumulating that this sort of wave-induced flow reversal in the bottom boundary layer is a prerequisite for the onset of global instability (Hammond & Redekopp 1998, Bogucki & Redekopp 1999, Wang & Redekopp 2001, Diamessis & Redekopp 2006). Based on the time series analyzed here, and the clear linkage between ISW packets and significantly enhanced concentrations of seabed particles at heights considerably above the nominal boundary layer, it is becoming increasingly evident that the ISW 'climate cycle' on coastal shelves is likely to exert a pivotal influence on both the fate of pollutants and on biological processes in these regions.

Acknowledgements

Support for this work was provided by the Office of Naval Research under Grant N00014-95-1-0041. We thank all researchers connected with the CMO project for their contributions to the success of the experiment. We are especially grateful to J. Barth, T. Dickey, M. Levine and J. Trowbridge

for making their data available for this work, and to S. Pierce for the tidal calculations. We thank M.-E. Carr for suggestions regarding the manuscript. We are also grateful to anonymous reviewers of an earlier version for their suggestions.

Appendix

Mode-1 and mode-2 ISW horizontal induced current

The properties of long linear internal waves in a general wave guide are given by the Taylor-Goldstein equation – see Maslowe & Redekopp (1980). The model KdV equation for CMO-like conditions has been solved in Wang et al. (2001). Here, in our model calculations we have taken a somewhat different environmental state: the upper stratified layer has a squared Brunt-Väisälä frequency $N^2(z) \simeq 10^{-3}$ s^{-2} and the underlying layer has a considerably weaker squared Brunt-Väisälä frequency $N^2(z) \simeq 10^{-4}$ s^{-2}.

For calculations we used the typical CMO observed mean current structure with the maximum value of 0.2 m s^{-1} at 35 mab and decreasing linearly towards zero at the bottom and decreasing linearly with the backflow layer near the surface. The vertical distribution of environmental parameters $U(z)$ and $N^2(z)$ is presented in Figure 3.

The ISW associated horizontal velocity (Wang et al. 2001) is presented in Figure 3. The current isolines are equally spaced – every 0.06 m s^{-1}.

In the calculations we used a mode-1 wave amplitude of 10 m (10–15 m typically in the CMO). For mode-2 we used the same ISW wave amplitude of 10 m observed in the experiment.

Note the difference between the mode-1 and mode-2 lengths; the overall longest wave is mode-1 upstream.

The mode-1 upstream/downstream waves induce the largest near-bottom currents of c. 0.15 m s^{-1}/ 0.1 m s^{-1} respectively. The mode-1 upstream propagating wave is generally broader in bottom-fixed reference coordinates and induces the longest lasting horizontal current. The mode-1 wave induces a near surface current speed of 0.6 m s^{-1}.

The mode-2 downstream wave induces a near-bottom current of

Figure 3. Top four panels: Comparison of the mode-1 and mode-2 upstream and downstream ISW induced currents. Bottom panel: The distribution of the environmental parameters $U(z)$ and $N^2(z)$. The model solution of the KdV equation for structure function is described in detail in Wang et al. (2001). Note the nearly tenfold difference between mode-1 and mode-2 ISW lengths. The mode-1 and mode-2 downstream waves can both increase the near-bottom current to 0.2 m s^{-1}. The current speed isolines are equally spaced – every 0.06 m s^{-1}

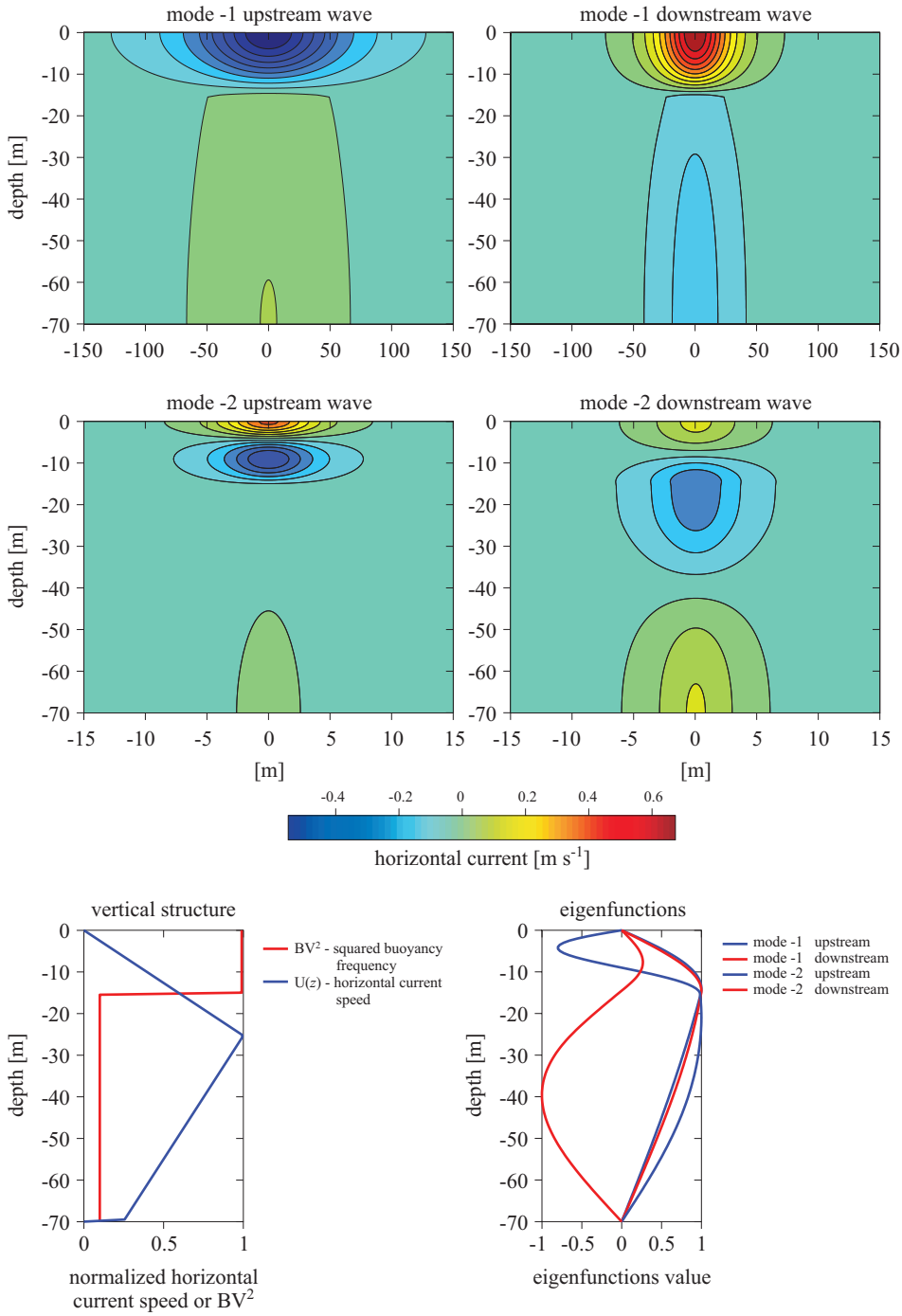
mode -1 upstream wave
mode -1 downstream wave
mode -2 upstream wave
mode -2 downstream wave
depth [m]
[m]
horizontal current [m s-1]
vertical structure
BV2 - squared buoyancy frequency
U(z) - horizontal current speed
normalized horizontal current speed or BV2
eigenfunctions
mode -1 upstream
mode -1 downstream
mode -2 upstream
mode -2 downstream
eigenfunctions value

Figure 3.

0.17 m s^{-1}, comparable to its mode-1 counterpart. This current for the mode-2 downstream is generated over a horizontal distance of 7.5 m, whereas for mode-1 this distance becomes 50 m/100 m for the downstream/upstream wave respectively. In addition, the mode-2 upstream generates an unprecedented upper layer shear attaining 0.08 s^{-1} within the upper 10 m of the water column.

The mode-2 upstream shear is larger than the mode-2 downstream shear of 0.03 s^{-1} within the upper 15 m and larger than the mode-1 downstream/upstream shear of 0.7 to 0.05 s^{-1} within the upper 15 m.

References

Bogucki D. J., Redekopp L. G., 1999, *A mechanism for sediment resuspension by internal solitary waves*, Geophys. Res. Lett., 26 (9), 1317–1320.

Bogucki D. J., Redekopp L. G., Barth J., 2005, *Internal solitary waves in the Coastal Mixing and Optics 1996 experiment: Multimodal structure and resuspension* J. Geophys. Res.-Oceans, 110 (C02024), 1–19.

Bogucki D. J., Redekopp L. G., Dickey T. D., 1997, *Sediment resuspension and mixing by resonantly generated internal solitary waves*, J. Geophys. Res.-Oceans, 27 (7), 1181–1196.

Boyd T., Levine M., Gard S. R., 1997, *SAR primer and CMO program*, Data report – Oregon State University, 164, p. 157.

Chang G. C., Dickey T. D., Williams A. J., 2001, *Sediment resuspension over a continental shelf during the hurricanes Edouard and Hortense*, J. Geophys. Res.-Oceans, 106 (C5), 9517–9532.

Diamessis P. J., Redekopp L. G., 2006, *Numerical investigation of solitary internal wave-induced global instability in shallow water benthic boundary layers*, J. Phys. Oceanogr., 36 (5), 784–812.

Dickey T. D., Chang G. C., Agrawal Y. C., Williams A. J., Hill P. S., *Sediment resuspension in the wakes of hurricanes Edouard and Hortense*, Geophys. Res. Lett., 25 (18), 3533–3536.

Grant W. D., Madsen O. S., 1986, *The continental-shelf bottom boundary layer*, Annu. Rev. Fluid Mech., 18, 265–305.

Hammond D. A., Redekopp L. G., 1998, *Local and global instability properties of separation bubbles*, Eur. J. Mech. B-Fluid., 17 (2), 145–164.

Hill P. S., Voulgaris G., Trowbridge J. H., 2001, *Control on floc size in a continental shelf bottom boundary layer*, J. Geophys. Res., 106 (C5), 9543–9550.

Johnson K. S., Chavez F. P., Friedrich G. E., 1999, *Continental-shelf sediment as a primary source of iron for coastal phytoplankton*, Nature, 398 (6729), 697–700.

MacKinnon J. A., Gregg M. C., 2005, *Near-inertial waves on the New England shelf: The role of evolving stratification, turbulent dissipation and bottom drag*, J. Phys. Oceanogr., 35 (12), 2408–2424.

Maslowe S., Redekopp L. G., 1980, *Long nonlinear waves in stratified shear flows*, J. Fluid Mech., 101, 321–348.

Na Y., Moin P., 1998, *Direct numerical simulation of a separated turbulent boundary layer*, J. Fluid Mech., 374, 379–405.

Redekopp L. G., 2002, *Elements of instability theory for environmental flows*, [in:] *Environmental stratified floes*, R. H. J. Grimshaw (ed.), Kluwer Acad. Publ., Boston, 225–281.

Saggio A., Imberger J., 1998, *Internal wave weather in a stratified lake*, Limnol. Oceanogr., 43 (8), 1780–1795.

Shaw W. J., Trowbridge J. H., 2001, *The direct estimation of near-bottom turbulent fluxes in the presence of energetic wave motions*, J. Atmos. Ocean. Tech., 18 (9), 1540–1557.

Shaw W. J., Trowbridge J. H., Williams A. J., 2001, *Budgets of turbulent kinetic energy and scalar variance in the continental shelf bottom boundary layer*, J. Geophys. Res., 106 (C5), 9551–9564.

Turnewitsch R., Graf G., 2003, *Variability of particulate seawater properties related to bottom mixed layer-associated internal waves in shallow water on a time scale of hours*, Limnol. Oceanogr., 48 (3), 1254–1264.

Wang B. J., Redekopp L. G., 2001, *Long internal waves in shear flows: topographic resonance and wave-induced global instability*, Dynam. Atmos. Oceans, 33 (4), 263–302.

Wang B. J., Bogucki D. J., Redekopp L. G., 2001, *Internal solitary waves in structured thermocline with implications for resuspension and the formation of thin particle-laden layers*, J. Geophys. Res., 106 (C5), 9565–9586.